npj | biofilms and microbiomes

Article

Published in partnership with Nanyang Technological University

https://doi.org/10.1038/s41522-025-00884-7

Clostridium scindens attenuates acute kidney injury by producing indole-3-acetic acid

Yi-zhi Cao[1,2,6], Jiang-yi Li[1,6], Jun-ming Hu[1,6], Ke Su[3], Jia-liang Chen[1], Ying Liu[4,7], Jia-Li Wei[5,7] & Zhi-hao Zhang[1,7] ✉

The association between gut microbiota and acute kidney injury (AKI) has garnered increased attention recently. Herein, we investigated the effect of the gut microbiota and its metabolites on regulating AKI-associated kidney injury and inflammation. We observed that *Clostridium scindens* (CS) can ameliorate ischemia/reperfusion injury/folic acid-induced renal dysfunction, oxidative stress, and inflammation, and enhance intestinal barrier function. Mechanistically, CS can facilitate indole-3-acetic acid (IAA) production via the tryptophan metabolic pathway: tryptophan–indole-3-pyruvic acid–IAA. The increased intestinal IAA activates the aryl hydrocarbon receptor to restore intestinal barrier integrity and decreases interferon-γ influx into the bloodstream, thereby alleviating renal inflammation. The natural product Nobiletin ameliorated AKI by promoting CS growth. Our findings suggest that regulating CS is a promising approach for treating AKI.

Acute kidney injury (AKI) is a common multifactorial disease affecting 10%–15% of hospitalized patients and more than 50% of patients in the intensive care unit[1]. AKI is closely associated with substantial short- and long-term morbidity and mortality in critically ill patients[2]. It causes renal injuries, increases serum creatinine and urinary protein levels, and decreases urine volume. Previous studies have revealed that AKI significantly increases the risk of subsequent progression to chronic kidney disease (CKD) in affected individuals[3]. To date, preventive strategies for AKI, including optimizing hemodynamic stability and volume status and avoiding nephrotoxic agents, constitute the cornerstone of early AKI management; however, kidney replacement therapy is the only therapeutic modality for severe AKI. Consequently, identifying novel and effective therapeutic strategies for AKI is urgently warranted.

Increasing evidence suggests a close relationship between intestinal microbiota and kidney diseases[4–6]. Research indicates the presence of gut dysbiosis, including the disturbance of *Escherichia coli*, *Bacteroidetes*, *Bifidobacterium*, *Salmonella*, *Lactobacillus*, *Clostridium*, *Ruminococcus*, *Rothia*, *Staphylococcus*, *Enterobacter*, *Faecalibacterium*, and *Lachnospiraceae*, in patients with AKI[7]. Treatment with *Bifidobacterium bifidum* FL228.1, FL276.1, and ZL.1 alleviates AKI by improving intestinal barrier function[8]. The intestinal colonization of *Parabacteroides goldsteinii* can ameliorate ischemia/reperfusion injury (IRI)-induced renal dysfunction, oxidative stress, apoptosis, and inflammation[9]. The oral administration of the probiotic *Limosilactobacillus reuteri* can help prevent lipopolysaccharide-induced AKI[10]. Overall, these findings suggest that supplementing specific intestinal bacteria can be a potentially new strategy for preventing and managing AKI.

Clostridium scindens (CS) represents an essential taxon within the human gut microbiota. Despite its low abundance, CS exerts a disproportionately profound effect on bile acid transformation and steroid metabolism within the mammalian gastrointestinal tract. A recent study has revealed that CS mitigates vancomycin-induced cholestasis and hepatic fibrosis by activating the FXR-FGF15/19 signaling pathway in the intestine[11]. Moreover, CS inhibits the growth and exotoxin expression of *Clostridioides difficile* in a bile acid-independent manner[12]. In our previous study, we observed a significant decrease in the abundance of CS in patients with CKD, and oral administration of CS ameliorates renal fibrosis in UUO/adenine-induced mice. However, whether treatment with CS can protect against AKI remains unknown. This study aimed to investigate whether CS mitigates AKI by modulating the gut-kidney axis through tryptophan-derived metabolites. Specifically, we sought to determine if CS alleviates

[1]Key Laboratory of Tropical Biological Resources of Ministry of Education and One Health Institute, School of Pharmaceutical Sciences, Hainan University, Haikou, China. [2]State Key Laboratory of Natural Medicines, Department of TCMs Pharmaceuticals, School of Traditional Chinese Pharmacy, China Pharmaceutical University, Nanjing, China. [3]Department of Nephrology, Renmin Hospital of Wuhan University, Wuhan, China. [4]Institute of Chinese Materia Medica & State Key Laboratory for Quality Ensurance and Sustainable Use of Dao-di Herbs, China Academy of Chinese Medical Sciences, Beijing, China. [5]Department of Nephrology, Hainan Affiliated Hospital of Hainan Medical University (Hainan General Hospital), Haikou, China. [6]These authors contributed equally: Yi-zhi Cao, Jiang-yi Li, Jun-ming Hu. [7]These authors jointly supervised this work: Jia-Li Wei, Ying Liu, Zhi-hao Zhang. ✉e-mail: zzh-198518@163.com

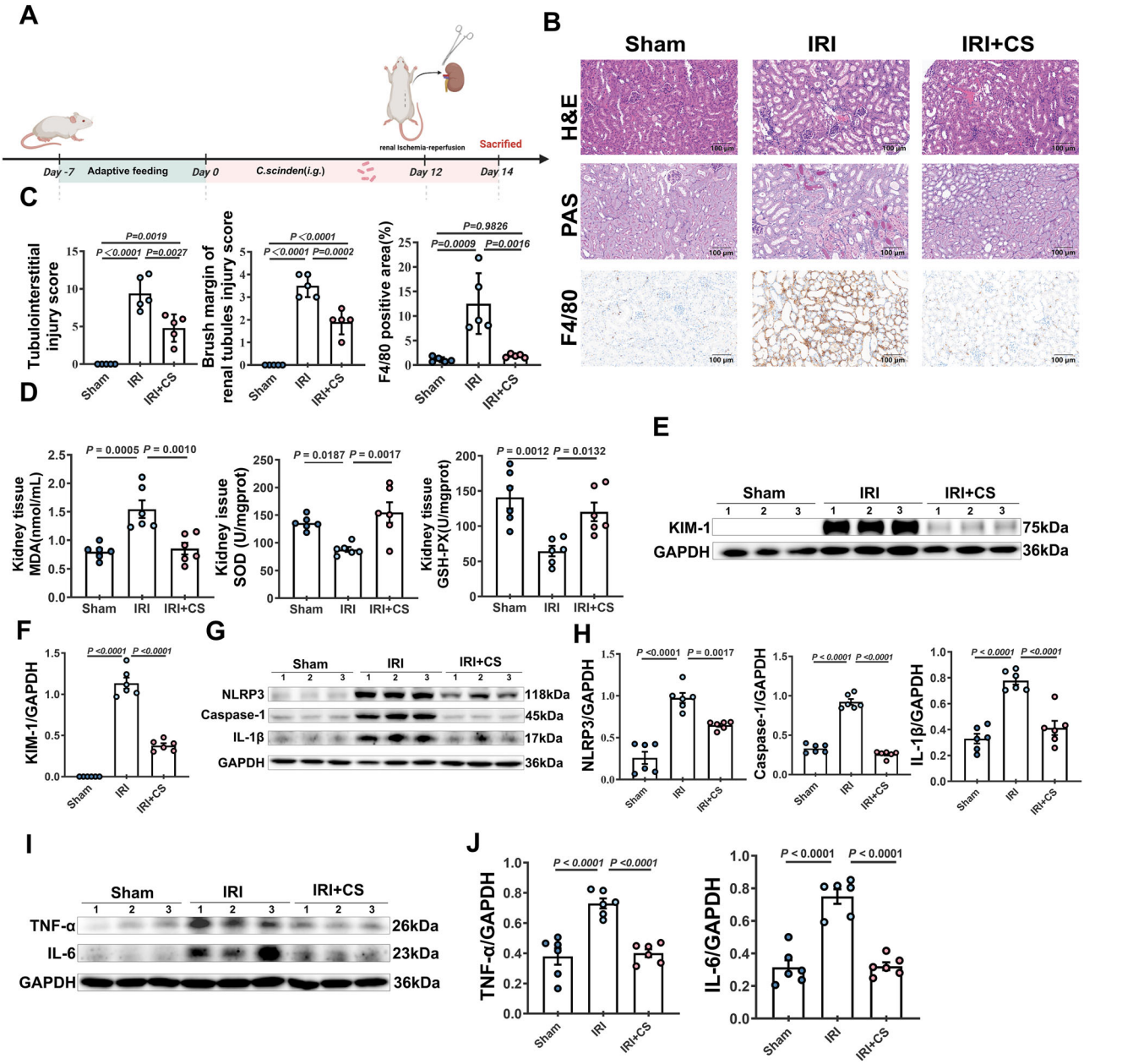

Fig. 1 | CS colonization ameliorates IRI-induced acute kidney injury. A Schematic diagram of CS treatment in the IRI animal model. **B** Representative H&E, PAS and F4/80 staining of the left kidney in different groups. **C** Quantification of Tubulointerstitial injury score, Brush margin of renal tubules and F4/80 positive area based on H&E staining, PAS staining and F4/80 staining ($n = 5$). **D** Quantification of MDA, SOD and GSH-PX levels in renal tissue of Sham, IRI, and IRI + CS group ($n = 6$). **E** Western blot analysis of kidney injury-related proteins in the left kidney of Sham, IRI, and IRI + CS group. **F** Quantification of KIM-1 protein expression from (**E**) ($n = 6$). **G** Western blot analysis of NLRP3 inflammasome-related protein expression in the kidneys of different groups. **H** Quantification of NLRP3、Caspase-1 and IL-1β protein expression from (**G**) ($n = 6$). **I** Western blot analysis of inflammatory pathway protein expression in the kidneys of different groups. **J** Quantification of TNF-α and IL-6 protein expression from (**I**) ($n = 6$).

renal injury by enhancing intestinal IAA production, activating the aryl hydrocarbon receptor to restore gut barrier function, and reducing systemic pro-inflammatory IFN-γ levels. Additionally, we explored the potential of the natural compound Nobiletin to amplify this protective mechanism by promoting CS growth. Our goal was to establish a foundation for novel therapeutic strategies targeting gut microbiota or their metabolites in AKI management.

Results

Gut colonization by CS attenuates IRI-induced AKI

To investigate the protective effect of CS on AKI, mice were orally administered CS for 12 consecutive days to colonize the gut (Fig. S3A). A mouse IRI model was constructed, with tissue collection at 48 h post-surgery (Fig. 1A). Hematoxylin-Eosin staining (H&E) and Periodic Acid-Schiff staining (PAS) staining revealed typical AKI-associated renal damage in the IRI group, with pathological changes such as interstitial inflammatory infiltration, tubular epithelial cell degeneration and necrosis, luminal exudate accumulation, loss of brush border, disorganized tubular architecture, and glomerular injury. F4/80 staining also revealed significant macrophage infiltration in the IRI group, which was mitigated by CS treatment. (Fig. 1B, C). These pathological changes were markedly alleviated in the IRI + CS group. Western blotting revealed elevated kidney injury molecule-1 (KIM-1) levels in IRI mice; the levels significantly decreased following CS treatment

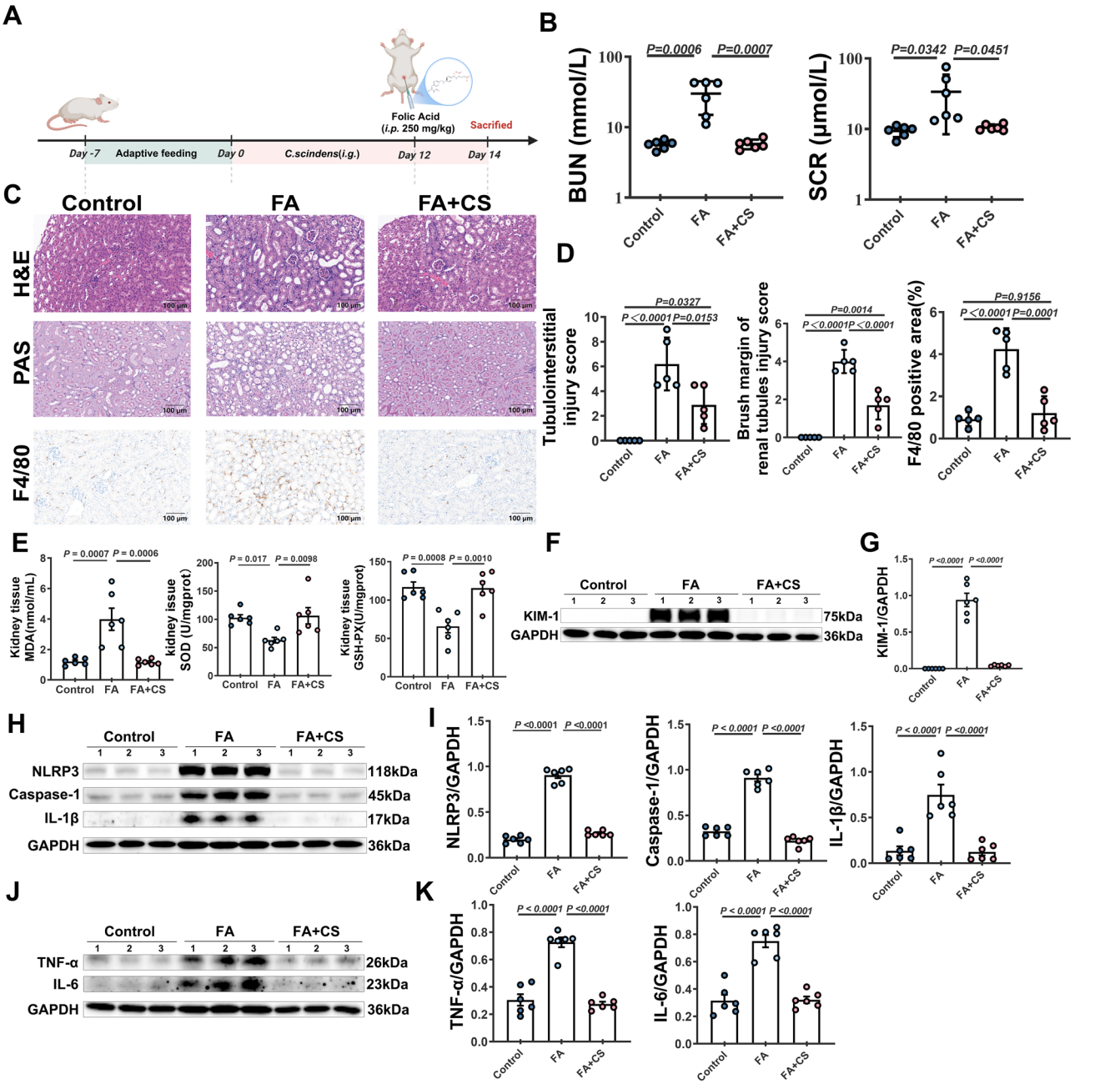

Fig. 2 | CS colonization ameliorates FA-induced acute kidney injury. A Schematic diagram of CS treatment in the FA animal model. **B** Serum Biochemical Levels of Scr and BUN in Each Group ($n = 6$). **C** Representative H&E, PAS and F4/80 staining of the left kidney in different groups. **D** Quantification of Tubulointerstitial injury score, Brush margin of renal tubules and F4/80 positive area based on H&E staining, PAS staining and F4/80 staining ($n = 5$). **E** Quantification of MDA, SOD and GSH-PX levels in renal tissue of Control, FA, and FA + CS group($n = 6$). **F** Western blot analysis of kidney injury-related proteins in the left kidney of Control, FA, and FA + CS group. **G** Quantification of KIM-1 protein expression from (**F**) ($n = 6$). **H** Western blot analysis of NLRP3 inflammasome-related protein expression in the kidneys of different groups. **I** Quantification of NLRP3、Caspase-1 and IL-1β protein expression from (**H**) ($n = 6$). **J** Western blot analysis of inflammatory pathway protein expression in the kidneys of different group. **K** Quantification of TNF-α and IL-6 protein expression from (**J**) ($n = 6$).

(Fig. 1E, F). Because oxidative stress is a key contributor to AKI progression, MDA, SOD, and GSH levels were measured. In IRI mice, MDA was significantly increased, whereas SOD and GSH were significantly decreased; CS treatment notably reversed the levels of these markers (Fig. 1D). Furthermore, we noted the strong activation of the NLRP3/Caspase-1 pathway in the IRI group, along with the increased expression of downstream inflammatory mediators (Fig. 1G–J). CS treatment suppressed this activation, indicating its anti-inflammatory potential. Collectively, these findings suggest that CS ameliorates AKI by decreasing oxidative stress and inflammation, preserving brush border integrity, and improving tubular function.

Colonization of CS alleviates folic acid-induced AKI

To further evaluate the therapeutic potential of CS in AKI, mice were colonized with CS via oral gavage (Fig. S3B), and a folic acid (FA)-induced AKI model was constructed (Fig. 2A). Figure 2B illustrates a significant increase in serum creatinine and blood urea nitrogen (BUN) levels in the FA group, indicating impaired glomerular filtration function. These levels were markedly decreased in the FA + CS group. Histological analysis revealed extensive inflammatory infiltration, tubular epithelial necrosis, luminal exudates and aggravated immunoinfiltration in the FA group (Fig. 2C, D); in contrast, significantly attenuated kidney injury, with smaller lesion areas and reduced inflammation, was noted in the FA + CS group. PAS staining

further revealed that FA administration resulted in brush border loss and glomerular damage, whereas CS treatment improved tubular morphology, decreased cast formation, and restored brush border integrity, suggesting enhanced structural recovery.

Biochemical analysis revealed that FA induced oxidative stress, characterized by increased MDA and decreased SOD and GSH levels; in contrast, CS treatment effectively reversed these changes (Fig. 2E). Western blotting revealed that KIM-1 was significantly upregulated in the FA group; this effect was markedly suppressed after CS administration (Fig. 2F, G). In addition, FA strongly activated the NLRP3 pathway, as evidenced by the increased expression of NLRP3, Caspase-1, and IL-1β (Fig. 2H, I), in addition to increased levels of the proinflammatory cytokines TNF-α and IL-6 (Fig. 2J, K). Treatment with CS inhibited the activation of the NLRP3 inflammasome and downregulated these inflammatory mediators, indicating its potent anti-inflammatory effect. Collectively, these findings suggest that FA-induced AKI is driven, in part, by NLRP3/Caspase-1 axis-mediated inflammation. CS colonization attenuates this response, decreases cytokine production, and alleviates kidney injury.

Analysis of gut microbiota structure and composition in IRI mice with CS treatment

We performed 16S rRNA sequencing of fecal samples from N, IRI, and IRI + CS treated mice. Principal coordinate analysis revealed a clear separation in gut microbiota between normal and AKI group, which was not significantly restored by CS treatment (Fig. S4A). The Chao1 index in different groups shows no statistically significant (Fig. S4B). At the genus level, heatmap analysis of differentially abundant bacteria demonstrated that IRI induced alterations in gut microbiota composition, characterized by reductions in *Dubosiella*, *Faecalibaculum*, and *Ligilactobacillus*, along with elevations in *Escherichia-Shigella*, *Parabacteroides*, and *Odoribacter* (Fig. S4C). Collectively, these findings indicate that while CS treatment confers renal protection, it does not mediate the whole restruction of the gut microbiota, but acts in a more direct way.

CS produces IAA in vitro

Our experiments revealed that CS colonization can effectively ameliorate AKI. Therefore, we hypothesized that CS exerts its protective effects by its metabolites. We subjected CS culture supernatants to untargeted metabolomic analysis to identify potential key metabolites involved in improving AKI. Principal component analysis of the metabolic profiles (Fig. 3A) revealed distinct separation between the blank medium group (CS Emp.) and the CS culture group (CS Sup.). This indicates significant metabolic changes in the supernatants following CS growth. Furthermore, we performed analysis in the positive ion mode and utilized orthogonal partial least squares discriminant analysis to identify significant metabolites based on variable importance in projection (VIP) values (VIP > 1, $P < 0.05$, fold change ≥ 2). In total, 13 significantly altered metabolites were identified, with 12 being upregulated and 1 being downregulated (Fig. 3B). The volcano plot and heat map visually displayed the metabolic changes. Tryptophan metabolism, closely associated with gut microbiota, is implicated in these changes[13]. We noted that IAA, a key metabolite in the tryptophan metabolism pathway, was elevated in CS-treated samples (Fig. 3B, C). By using the IAA standard, we further confirmed that IAA levels were significantly higher in CS culture supernatants than in the blank medium. These findings suggest that CS produces IAA in vitro (Fig. 3D).

CS metabolizes tryptophan to IAA via indole-3-pyruvic acid

To investigate the metabolic pathway of IAA production in CS, we hypothesize that CS uses the same metabolic routes for IAA as in humans (Fig. 3E). Then, we used deuterated tryptophan (D5-Tryptophan, D5-Try) as starting materials to trace its metabolism in CS. As shown in Fig. 3F, G, after the administration of D5-Try, D5-indole-3-pyruvic acid (D5-IPA) and D5-indole-3-acetic acid (D5-IAA) were significantly increased, whereas D5-indole-3-acetamide (D5-IMA) was not detected in CS culture supernatants. Furthermore, all these metabolites, including D5-IPA, D5-IAA, and D5-IMA, were not detected in heat-inactivated CS culture supernatants. These results suggest that CS can metabolize tryptophan into IPA and IAA but not into IMA. Next, we investigated whether CS can convert D5-IPA into D5-IAA (Fig. 3G). After the administration of D5-IPA, D5-IAA levels increased in CS culture supernatants; however, D5-IAA was not detected in heat-inactivated CS culture supernatants. This suggests that CS can convert D5-IPA to D5-IAA. Subsequently, D5-IMA was used as a precursor, and D5-IAA was not detected in CS culture supernatants, indicating that CS cannot convert D5-IMA into D5-IAA. In addition, using indole-3-acetaldehyde (IAC) as a precursor (Fig. 3H), we observed an increase in IAA, suggesting that CS can convert IAC to IAA. Collectively, we demonstrate that CS metabolizes tryptophan into IPA, which is further converted into the final product, IAA (Fig. 3I).

CS regulates IFN-γ and tight junction integrity to alleviate AKI

Our experiments revealed that CS can metabolize tryptophan into IAA. To investigate the changes in IAA levels, we analyzed IAA content in fecal and serum samples of the Sham, IRI, and IRI + CS groups (Fig. 4A). Fecal IAA levels were decreased in the model group but increased in the IRI + CS group. Although serum IAA levels were detectable, no significant changes were noted. This indicates that IAA primarily exerts its effects within the gut.

To further explore how CS colonization affects gut inflammation, colon tissues were subjected to protein microarray analysis to measure 31 common chemokines. IFN-γ was the only chemokine significantly upregulated in the IRI model, which was downregulated after CS treatment (Fig. 4B). IFN-γ has been implicated in promoting antigen presentation, suppressing inflammasome activation, and regulating T cell activation and proinflammatory cytokine production[14,15]. We hypothesize that IFN-γ plays an essential role in mediating AKI severity. qPCR analysis revealed that IFN-γ expression was significantly upregulated in the colon in both IRI and FA-induced AKI models; in contrast, CS treatment notably decreased its gene expression (Fig. 4C). These findings suggest that CS treatment, by increasing IAA levels in the gut, downregulates IFN-γ expression, thereby modulating inflammation in AKI. In addition, we measured serum IFN-γ levels, which were significantly increased in both AKI models. However, treatment with CS significantly decreased these elevated levels (Fig. 4D). To evaluate intestinal tight junction integrity, we subjected colon tissues to western blotting. We observed that AKI significantly decreased tight junction protein levels, which were restored after CS treatment (Fig. 4E–H). To further investigate the mechanism of IFN-γ in AKI, we neutralized it in the model of IRI using the specific antibody XMG 1.2. The results demonstrated that IFN-γ neutralization not only ameliorated kidney injury but also attenuated the inflammatory response, producing a protective effect comparable to CS treatment (Fig. 4I–M). Collectively, AKI disrupts intestinal tight junctions, allowing IFN-γ to enter the bloodstream. CS decreases IFN-γ expression and enhances tight junction integrity, decreasing systemic IFN-γ levels, thereby alleviating renal inflammation. Importantly, neutralizing IFN-γ during AKI exerts a protective effect comparable to that of CS treatment.

IAA modulates AhR receptor activation to restore intestinal tight junctions in AKI

To explore the mechanism by which CS restores intestinal tight junctions, we focused on AhR, a known IAA receptor, in regulating gut barrier function. Existing literature suggests that intestinal barrier disruption suppresses AhR receptor activity, whereas AhR activation helps restore tight junction integrity[16]. In vitro, we utilized Caco-2 cells to induce intestinal injury using LPS as an inducer, followed by the addition of IAA or the AhR inhibitor (CH-233191) to assess their effects on tight junctions. As illustrated in Fig. 5A, B, LPS treatment significantly decreased the expression of ZO-1 and Occludin by reducing the expression of AhR, indicating that the compromise of tight junctions is associated with impaired AhR signaling. Disruption of intestinal tight junctions increased serum IFN-γ levels (Fig. 4D), and IFN-γ can induce inflammation of HK-2 cells (Fig. 5C).However, IAA treatment restored ZO-1 and Occludin expression; this effect was reversed by CH-233191. In addition, LPS treatment decreased

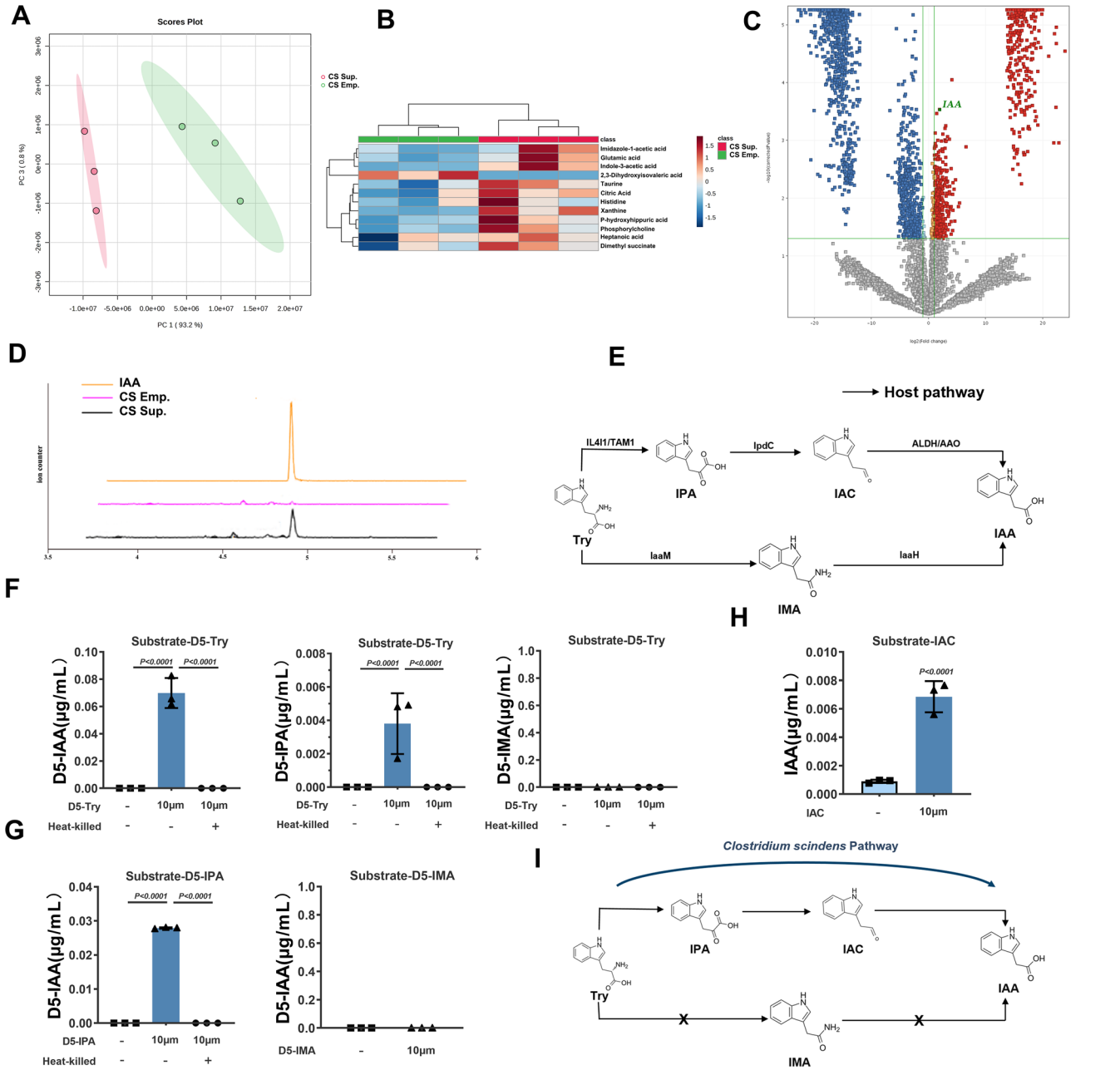

Fig. 3 | CS metabolize tryptophan in vitro. A PCA analysis of metabolites from CMC medium (CS Emp. group) and CS supernatant (CS Sup. group) ($n = 3$). **B** Heatmap of selected significantly different metabolites between CS Emp. group and CS Sup. group. **C** Volcano plot analysis of metabolites from CS Emp. group and CS Sup. group. **D** EIC spectra analysis of different groups. **E** Tryptophan metabolism pathway in humans. **F** After 24 h of D5-Try treatment, the levels of D5-IAA, D5-IPA, and D5-IMA in the solution were measured($n = 3$). **G** After resuspending CS in PBS, the solution was supplemented with differrent precursors (D5-IPA and D5-IMA) and D5-IAA levels were measured after 24 hours ($n = 3$). **H** After resuspending CS in PBS, the solution was supplemented with the precursor IAC, and IAA levels were measured after 2 h ($n = 3$). **I** Tryptophan metabolism pathway of CS in vitro.

AhR protein levels, whereas IAA treatment significantly enhanced AhR levels. CH-233191 reversed the effect of IAA on AhR. In the IRI and FA models, we further validated AhR upregulation in colon tissues. CS colonization significantly upregulated AhR expression (Fig. 5D, E, S5A, 5B). At the gene level, *AhR* and its downstream target gene *Cyp1A1* were significantly downregulated in the model group; in contrast, CS colonization upregulated the expression of both *Ahr* and *Cyp1A1* (Fig. 5F, S5C). To further clarify the role of intestinal AhR in regulating AKI, we employed CH-223191-loaded nanoparticles for intestine-specific delivery to inhibit AhR activation and evaluated their impact in on CS treatment. The results demonstrated that treatment with CH-223191-loaded postbiotic nanoparticles reverse the renoprotective effects of CS on intestine, and thereby reversing the amelioration of renal injury and inflammation. (Fig. 5G–K, S5D, S5E). These findings suggest that CS colonization or IAA administration restores intestinal tight junction integrity and reducing inflammation by activating the intestinal AhR receptor, playing an essential role in the recovery from AKI.

Nobiletin ameliorates IRI-induced AKI in a gut microbiota-dependent manner

We have noted that CS can significantly ameliorate AKI. Therefore, we hypothesized that active compounds in traditional Chinese medicine can attenuate AKI by acting on CS. Nobiletin, a flavonoid found in citrus fruits, can reduce ferroptosis in sepsis-induced liver injury by modulating the gut

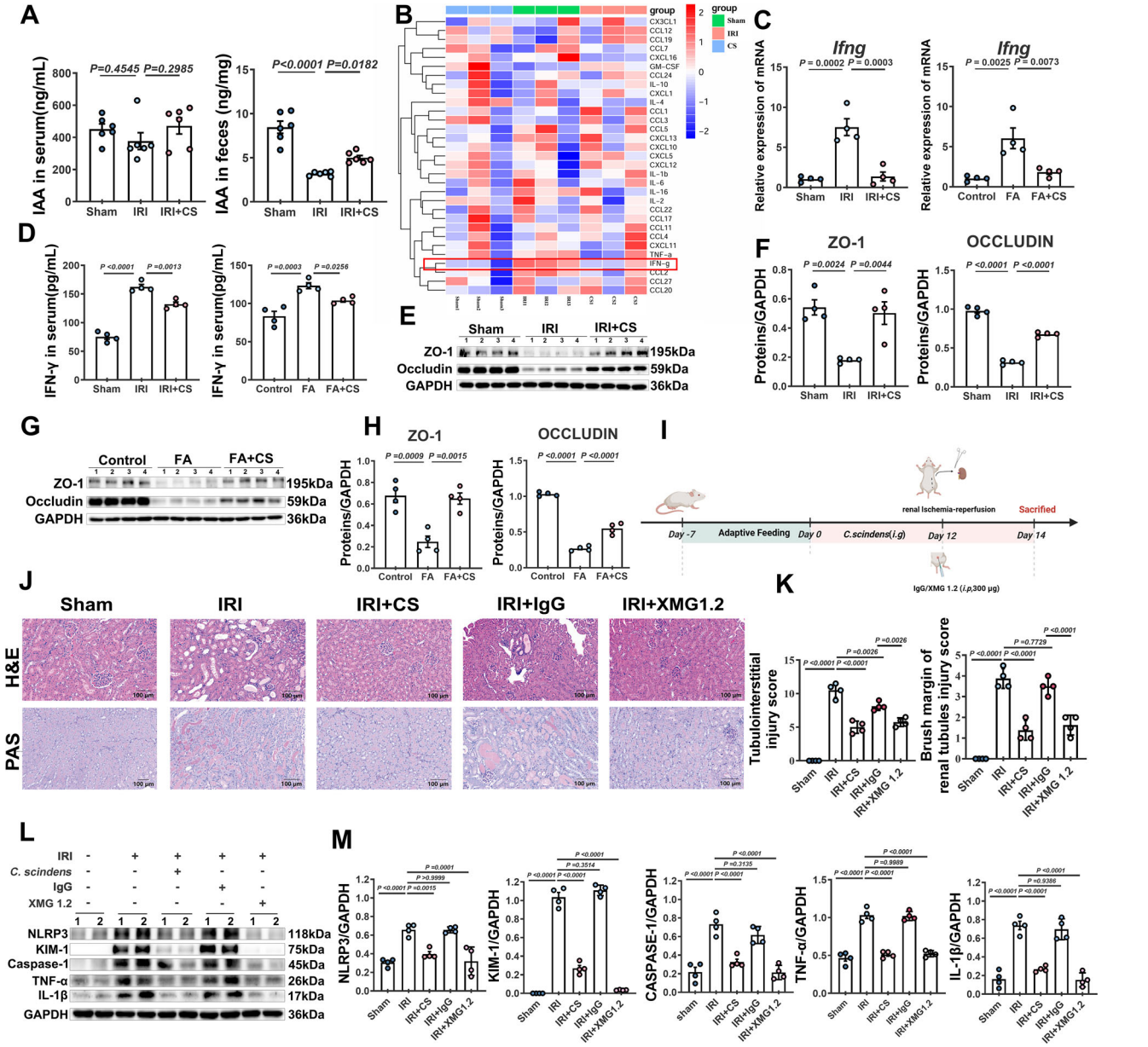

Fig. 4 | Effects of CS on IAA levels, cytokine expression, and intestinal barrier integrity in AKI models. A Quantification of IAA levels in various tissues from the Sham, IRI, and IRI + CS group ($n = 6$). **B** Heatmap analysis of cytokine expression in the colon based on protein microarray results in the Sham, IRI, and IRI + CS group ($n = 3$). **C** qPCR analysis of IFN-γ expression in colonic tissues from different groups ($n = 4$). **D** Cytokine quantification of IFN-γ levels in serum samples from each group ($n = 4$). **E** Representative Western blot images of intestinal tight junction proteins (ZO-1 and Occludin) in the Sham, IRI, and IRI + CS group ($n = 4$). **F** Densitometric quantification of ZO-1 and Occludin expression from (**E**). **G** Representative Western blot images of ZO-1 and Occludin in intestinal tissues from the Control, FA, and FA + CS group ($n = 4$). **H** Densitometric quantification of ZO-1 and Occludin expression from (**G**). **I** Schematic diagram of the experimental strategy for in vivo antibody neutralization in mice. **J** Representative H&E and PAS staining of the left kidney in different groups. **K** Quantification of Tubulointerstitial injury score and Brush margin of renal tubules based on H&E staining and PAS staining ($n = 4$). **L** Western blot analysis of kidney injury-related proteins in the left kidney of Sham, IRI, IRI + CS, IRI + IgG and IRI + XMG 1.2 group. **M** Quantification of KIM-1、NLRP3、Caspase-1, and IL-1β and TNF-α protein expression from panel L($n = 4$).

microbiome[17–19]. Moreover, ferroptosis is closely associated with AKI. Proanthocyanidins are known for their antidiabetic effects and ability to improve metabolism. Both compounds were considered for their potential to modulate gut microbiota, particularly beneficial bacteria. Therefore, we speculated that Nobiletin and proanthocyanidins may promote the growth of CS. In vitro experiments revealed that Nobiletin promoted CS growth at a concentration of 10 μM; however, proanthocyanidins did not significantly affect CS growth (Fig. 6B, Fig. S2). Meanwhile, Nobiletin also increases the abundance of CS in vivo (Fig. S3C, S3D). H&E and PAS staining revealed significant renal injury in the IRI group, with pathological changes such as glomerular atrophy, tubular vacuolar degeneration, cellular flattening, and severe inflammatory cell infiltration (Fig. 6C, D). In contrast, these injuries were significantly alleviated in the Nobiletin-treated group. Treatment with Nobiletin substantially decreased the expression of KIM-1, a kidney injury marker (Fig. 6F, G). Furthermore, we explored the effects of Nobiletin on oxidative stress and the NLRP3/Caspase-1 inflammasome pathway. Nobiletin treatment significantly decreased MDA but enhanced SOD and GSH levels (Fig. 6E). In addition, Nobiletin treatment attenuated NLRP3 pathway activation, as evidenced by decreased NLRP3, Caspase-1, and IL-1β expression in kidney tissues (Fig. 6H, I). Moreover, Nobiletin significantly suppressed the expression of the proinflammatory cytokines TNF-α and IL-6, which were elevated in the IRI model (Fig. 6J, K). Finally, we observed that

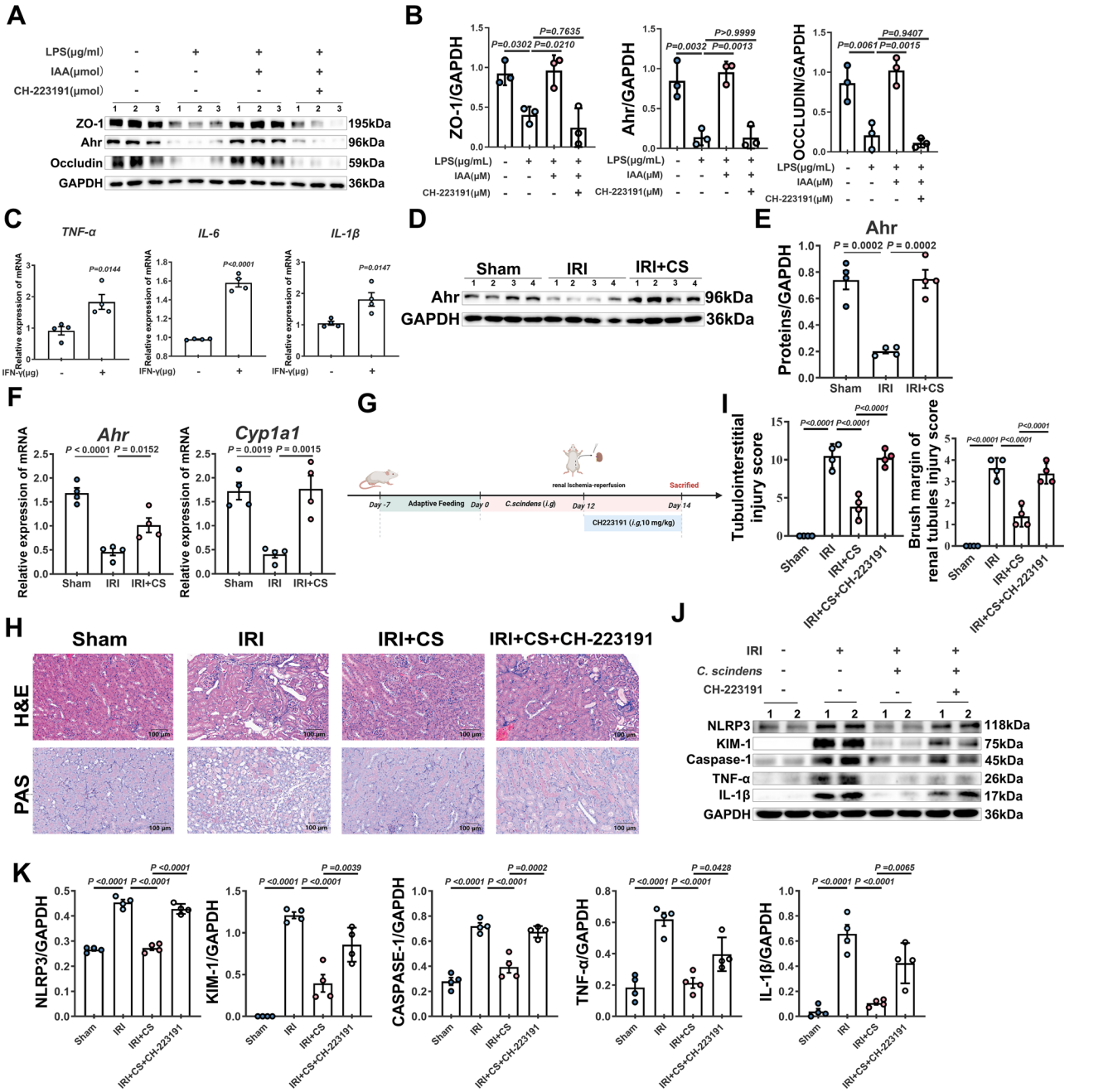

Fig. 5 | Role of AhR signaling in intestinal and renal crosstalk mediated by IAA. **A** The expression levels of ZO-1, Occludin and AhR in Caco-2 cells were measured using western blotting after HK-2 cells were treated with IAA, or with a combination of IAA and CH-233191, followed by stimulation with 100 μg/mL LPS for 24 h. **B** Quantitative analysis based on data from (**A**) ($n = 3$). **C** The expression levels of *TNF-α*、*IL-6*, and *IL-1β* in HK-2 cells were measured by qPCR after HK-2 cells were treated with or without IFN-γ for 24 hours($n = 4$). **D** Representative Western blot images showing AhR activation in colonic tissue from the Sham, IRI, and IRI + CS group. **E** Quantitative analysis of AhR protein expression from (**D**) ($n = 4$). **F** Relative mRNA expression levels of *Ahr* and *Cyp1a1* in colonic tissue from the Sham, IRI, and IRI + CS group, assessed by qPCR ($n = 4$). **G** Schematic diagram of nanoparticle-based Inhibition of intestinal AhR in the CS-Treated IRI Model. **H** Representative H&E and PAS staining of the left kidney in different groups. **I** Quantification of Tubulointerstitial injury score and Brush margin of renal tubules based on H&E staining and PAS staining ($n = 4$). **J** Western blot analysis of kidney injury-related proteins in the left kidney of Sham, IRI, IRI + CS and IRI + CS + CH-223191 group. **K** Quantification of KIM-1、NLRP3、Caspase-1 and IL-1β and TNF-α protein expression from (**J**) ($n = 4$).

AhR levels were decreased in the colon and intestinal tight junctions, which were compromised in the model group. However, treatment with Nobiletin significantly upregulated AhR levels and restored intestinal tight junction integrity (Fig. 6L, M). To investigate whether the renoprotective effects of Nobiletin depend on the presence of gut microbiota, we treated IRI mice with a cocktail of antibiotics. We noted that when the antibiotic cocktail suppressed the gut microbiota, the renoprotective effects of Nobiletin were abolished (Fig. 6C–M).

Nobiletin improves FA-induced AKI in a gut microbiota-dependent manner

We demonstrated that Nobiletin effectively ameliorates kidney injury in the IRI model and that this effect partially depends on the gut microbiota. To confirm this investigation, we explored the effects of Nobiletin in the FA-induced AKI model. As illustrated in Figs. S6C, S6D, FA treatment significantly damaged the kidney, with pathological changes such as glomerular atrophy, tubular dilation, necrosis, and cast formation. Nobiletin

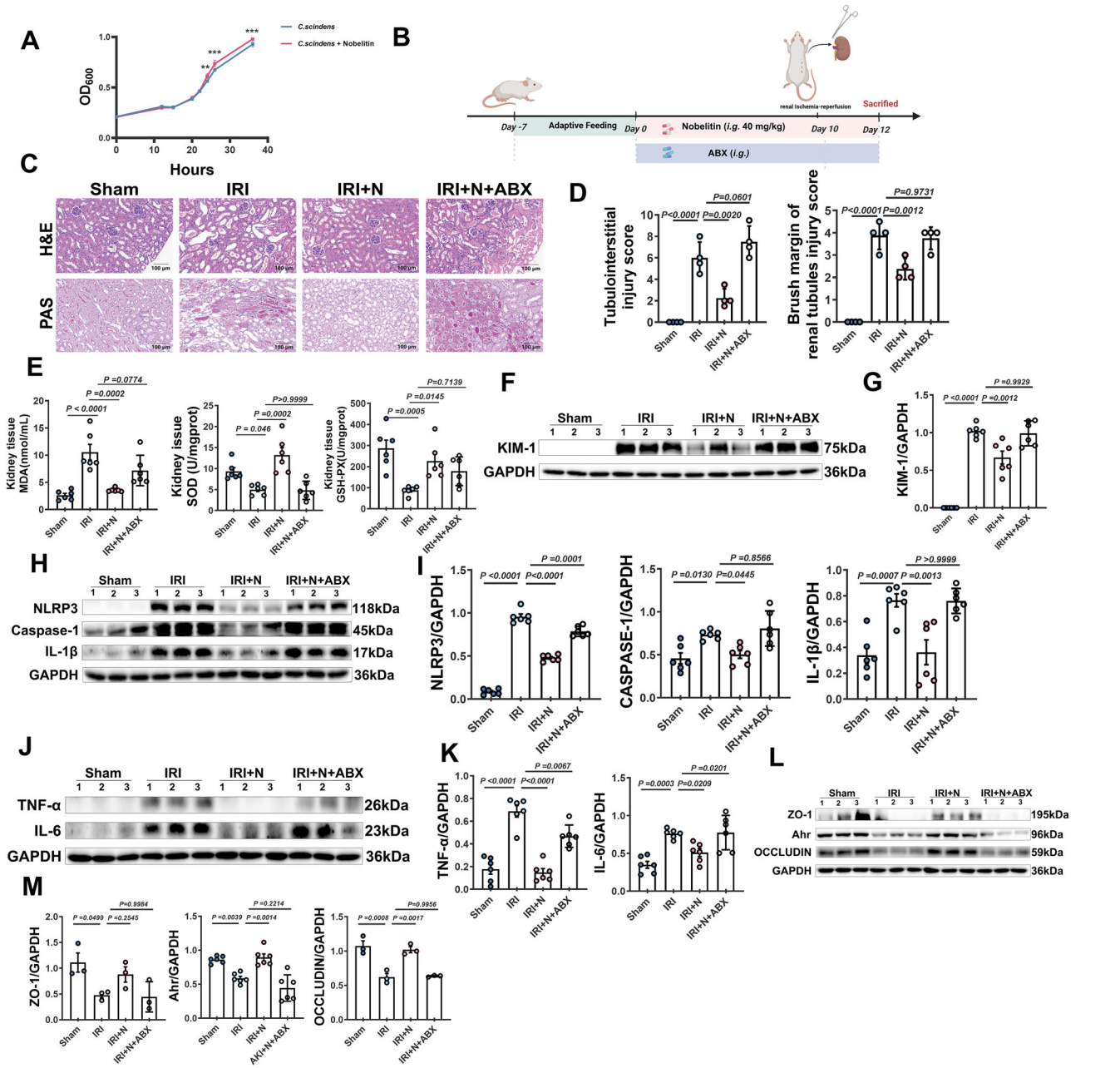

Fig. 6 | Nobiletin ameliorates IRI-induced acute kidney injury via modulating gut microbiota. **A** Growth curve of CS treated with Nobiletin. **B** Schematic diagram of the experimental process for Nobiletin treatment in the IRI animal model. **C** Representative H&E and PAS staining of the left kidney in different groups. **D** Quantification of Tubulointerstitial injury score and Brush margin of renal tubules injury score based on H&E and PAS staining ($n = 4$). **E** Quantification of MDA, SOD and GSH-PX levels in renal tissue of Sham, IRI, IRI + N and IRI + N + ABX group ($n = 6$). **F** Western blot analysis of kidney injury-related proteins in the left kidney of Sham, IRI, IRI + N and IRI + N + ABX group. **G** Quantification of protein expression from (**F**) ($n = 6$). **H** Western blot analysis of NLRP3 inflammasome-related protein expression in the kidneys of different groups. **I** Quantification of NLRP3、Caspase-1 and IL-1β protein expression from (**H**) ($n = 6$). **J** Western blot analysis of inflammatory pathway protein expression in the kidneys of different groups. **K** Quantification of TNF-α and IL-6 protein expression from (**J**) ($n = 6$). **L** The expression levels of Intestinal tight junction protein in the colonic tissue of Sham, IRI, IRI + N and IRI + N + ABX group. **M** Quantification of ZO-1 ($n = 3$), Occludin ($n = 3$) and AhR ($n = 6$) protein expression from (**L**).

treatment alleviated tubular dilation, decreased cast formation, and restored the brush border. Scr and BUN levels were significantly increased in the FA group, indicating impaired glomerular filtration; In contrast, kidney function was improved in the Nobiletin group (Fig. S6B). FA also induced oxidative stress, marked by increased MDA and decreased SOD and GSH levels (Fig. S6E). Nobiletin treatment significantly reversed the levels of these markers, although antibiotic treatment counteracted these effects. KIM-1 expression was increased in the FA group, which was significantly downregulated in the Nobiletin-treated group (Fig. S7F, 7G). However, in the antibiotic-treated group, KIM-1 expression did not significantly decrease. The NLRP3/Caspase-1 pathway was significantly activated in the FA group. Nobiletin treatment markedly suppressed this activation (Figs. S6H, S 6I), whereas the suppression of NLRP3 was less pronounced in antibiotic-treated mice. In addition, Nobiletin treatment significantly decreased the levels of the proinflammatory cytokines TNF-α and IL-6 in the FA group (Figs. S6J, S6K). However, antibiotic treatment diminished this effect. Finally, consistent with previous results, we observed decreased AhR levels and compromised intestinal tight junctions in the FA group. Nobiletin

treatment restored AhR expression and significantly improved tight junction integrity; however, the effect was reversed by the antibiotic depletion of gut microbiota (Figs. S6L, S6M). Collectively, Nobiletin improves kidney function in FA-induced AKI mice by decreasing oxidative stress and inflammation and restoring intestinal tight junctions in a gut microbiota-dependent manner.

Discussion

The gut microbiota plays an essential role in the pathogenesis of AKI[20]. Several studies have highlighted its effect on the systemic immune response, inflammatory pathways[20,21], and oxidative stress[22]. Gut microbial metabolites, including short-chain fatty acids (SCFAs) and IPA, play a protective role in kidney function. SCFAs can exert anti-inflammatory and antioxidative effects, which are essential for decreasing kidney damage during AKI[23,24]. While IPA restores SIRT1 function, it enhances PGC-1α activity, mitochondrial biosynthesis, and antioxidant defense, thereby attenuating diabetic kidney disease[25]. In the present study, we noted that CS treatment could effectively alleviate renal histopathological damage induced by IRI/FA in mice and improve kidney function.

CS has emerged as a potential probiotic with therapeutic effects in several diseases. CS can regulate gut microbiota by converting bile acids, particularly via 7α-dehydroxylation, to produce secondary bile acids, thereby affecting gut metabolism[26]. In addition, CS modulates the expression of G-protein-coupled bile acid receptor 5 by producing deoxycholic acid, alleviating renal fibrosis and CKD progression[6]. Beyond its role in regulating gut microbiota, CS also enhances the host's immune response, particularly against *Clostridium difficile* infections[27]. These findings suggest that CS exhibits broad potential in regulating metabolism and immune responses, making it a promising probiotic candidate for improving kidney health and managing AKI. In the present study, we demonstrated that CS treatment significantly increases IAA levels in the gut, which modulates the intestinal immune microenvironment and inflammation. In particular, CS-induced IAA production alleviates AKI by regulating IFN-γ levels and improving tight junction integrity in the intestines.

Researchers are increasingly recognizing the beneficial role of tryptophan metabolites in various diseases. For example, Wei Du et al. have reported that 5-hydroxyindole-3-acetic acid, a tryptophan metabolite, can activate AhR, improve insulin signaling in the liver, and suppress mTORC1 signaling, which together enhance glucose tolerance and alleviate obesity in high-fat diet-fed mice while maintaining liver insulin sensitivity[28]. Similarly, IAA and short-chain fatty acids are essential in protecting endothelial barriers, possibly offering potential protection in CKD by preventing epithelial barrier disruption. Microbial remodeling of gut tryptophan metabolism and indole-3-lactate production revealed that they regulate epithelial barrier repair and viral suppression in human and simian immunodeficiency virus infections[29]. IAA administration partially reversed Western diet-induced changes in the hepatic metabolome and proteome, specifically downregulating the expression of several enzymes in hepatic lipogenesis and β-oxidation[30]. The plant hormone indole-3-acetic acid derivative mitochonic acid 5 can bind to the mitochondrial inner membrane protein mitofilin and promote the regeneration of adenosine triphosphate. Furthermore, it can play a role in IRI and cisplatin-induced AKI mouse models[30]. These studies suggest that tryptophan metabolites, particularly IAA, may exert significant therapeutic potential in various diseases, including kidney diseases, by regulating immune responses and maintaining cellular integrity. In our study, we identified the specific metabolic pathways of IAA in CS. This type of bacteria can metabolize tryptophan. Through the tryptophan–IPA–IAA metabolic axis, it increases IAA levels in the intestinal tract. IAA activates AhR in the intestinal tract, regulates intestinal inflammation and barrier function, and further promotes kidney protection. Notably, although we demonstrated that CS can metabolize tryptophan to IAA, indole-3-aldehyde was not detected in our in vitro conversion experiments. Moreover, adding exogenous indole-3-aldehyde can produce IAA; however, its yield is low. The reason for this phenomenon is very likely owing to the instability of indole-3-aldehyde. Most of the indole-3-aldehyde was degraded before being converted to IAA.

AhR is a well-known ligand-activated transcription factor that modulates the expression of various genes involved in immune regulation[31,32] and barrier integrity[33]. AhR activation can improve intestinal tight junctions, which are essential for maintaining gut barrier function and preventing systemic inflammation[33]. In the context of AKI, we noted that CS treatment activates AhR signaling in the intestine, restoring tight junction proteins and decreasing systemic inflammation, both of which contribute to alleviating kidney injury. The disruption of tight junctions in the intestines allows inflammatory mediators, including IFN-γ, to leak into the bloodstream, exacerbating kidney damage. By restoring tight junction integrity, CS prevents this harmful leakage and decreases systemic inflammation.

IFN-γ is a proinflammatory cytokine that exacerbates kidney injury by inducing cellular stress and promoting immune cell infiltration[34]. Under the condition of hypertension, $CD4^+$ and $CD8^+$ T cells accumulate in the kidney. $CD8^+$ T cells release prohypertensive cytokines, such as TNF-α and IFN-γ, with T cell activation. These cytokines then induce increased expression of sodium transporters and renal vasoconstriction, ultimately leading to reduced renal blood flow and promoting fluid retention[35]. It has been reported that treatment with granulocyte-macrophage colony-stimulating factor (GM-CSF) and IFN-γ differentiated myeloid-derived suppressor cells (MDSCs) in vitro. When these differentiated MDSCs were transplanted into IRI mice, an increase in the numbers of macrophages and dendritic cells was observed. This change may increase renal injury and damage renal function, contributing to the early phase of IRI[36]. In addition, both IL-17A and IFN-γ act synergistically to recruit neutrophils to the injured kidney following damage[37]. Collectively, these studies indicate that elevated levels of IFN-γ may be a key driver of pathological changes in the kidney. In the present study, we noted that IFN-γ induces inflammation in HK-2 cells. Moreover, treatment with CS decreases IFN-γ levels in the intestine and serum, further supporting the role of CS in regulating immunity and inflammation during AKI. We found that following IFN-γ neutralization, the inflammatory response linked to AKI was significantly reduced. Importantly, this reduction in inflammation exhibited similar effects to those seen with CS colonization. Thus, we conclude that either CS colonization or via specific neutralizing antibodies may offer valuable insights for the treatment and prevention of acute kidney injury.

Nobiletin enhanced CS abundance in the gut, thereby potentiating its therapeutic effects. By increasing CS levels, Nobiletin boosted CS-mediated reductions in oxidative stress, inflammation, and kidney injury. The efficacy of Nobiletin was diminished when gut microbiota was depleted, confirming that its actions partially depend on a healthy microbiome. These results emphasize the importance of modulating gut microbiota, particularly CS, in AKI treatment. In summary, our findings suggest that CS and Nobiletin treatment protect against AKI via distinct yet complementary mechanisms involving gut microbiome modulation, oxidative stress regulation, inflammation suppression, and tight junction restoration.

In this study, we identified a specific metabolic pathway for IAA within CS. This bacterium metabolizes tryptophan to produce IAA, which may activate AhR and modulate gut inflammation and barrier function, decrease the level of IFN-γ in serum, and further contributing to kidney protection. Our findings underscore the complexity of tryptophan metabolites in kidney diseases and suggest that additional investigation into these metabolic pathways can provide novel therapeutic targets for clinical treatments. CS treatment significantly alleviated kidney injury in both IRI- and FA-induced AKI models. CS treatment improved kidney function by alleviating oxidative stress and inflammation and restoring tight junction integrity.

Although our study demonstrates the renal protective effects of CS in AKI and reveals its metabolic capacity for IAA production, several limitations should be acknowledged. First, the precise enzymatic machinery in CS responsible for tryptophan-to-IAA conversion remains uncharacterized.

Future work should focus on identifying the specific genes and enzymes involved in this pathway. Second, all experimental evidence was derived from animal models, which may not fully recapitulate pathophysiology of AKI in humans. Further validation in clinical cohorts is needed to assess the translational relevance of our findings. Third, while our data support the involvement of the IAA-AhR axis, the direct cellular mechanisms in renal cells remain incompletely resolved. Future studies using germ-free mice, renal organoids, and human tissue samples will help clarify the precise role of IAA in kidney protection and its therapeutic potential in AKI.

Methods

Mouse models

All animal experiments were conducted at the Experimental Animal Center of the School of Pharmacy, Hainan University (Haikou, China). The study protocols were approved by the Animal Ethics Committee of the School of Pharmacy, Hainan University (Ethics Approval No. HPIACUC2024081), and all procedures were performed in accordance with the Guide for the Care and Use of Laboratory Animals. Male Institute of Cancer Research (ICR) mice, weighing 18–20 g and of the same genotype, were randomly assigned to different treatment groups. All animals were housed in specific pathogen-free (SPF) facilities under controlled temperature and humidity, with free access to food and water. Following approval by the Laboratory Animal Use and Management Committee of the School of Pharmacy, Hainan University, mice were euthanized by cervical dislocation at the completion of the experiment. Blood was collected, and tissues were harvested and immediately stored at −80 °C until further analysis.

Cell culture

HK-2 cells were cultured in DMEM/F12 medium supplemented with 10% fetal bovine serum (FBS) and 1% penicillin–streptomycin at 37 °C in a humidified atmosphere containing 5% CO_2.

Caco-2 cells were cultured separately in complete culture medium (CM-0050, purchased from Procell Life Science & Technology Co., Ltd., China) and maintained under the same conditions (37 °C, 5% CO_2).

IRI model

Male mice were divided into Sham, IRI, and IRI + CS groups ($n = 8$ per group). Mice were anaesthetised by inhalation of isoflurane, a midline abdominal incision was made to expose the kidneys. The left renal artery was clamped for 45 minutes to induce ischemia, while saline-soaked gauze was applied to maintain kidney moisture. Reperfusion was initiated by removing the clamps, and the incision was sutured. Sham-operated mice underwent the same procedure without arterial clamping. Mice in the IRI + CS group received oral gavage of CS (0.2 mL, 10^8 CFU/mL) once daily for 14 days, beginning 12 days prior to surgery.

CH-223191-postbiotics nanoparticles were prepared according to the method described in the literature[38]. Mice were divided into four groups: Sham, IRI, IRI + CS, and IRI + CS + CH-223191 ($n = 8$ per group). The IRI + CS + CH-223191 group received daily oral gavage of CH-223191-postbiotic nanoparticles (100 mg/kg) after surgery, a dose that delivers an effective final concentration of approximately 10 mg/kg in the intestinal lumen.

In a separate experiment, mice were assigned to Sham, IRI, IRI + Nobiletin, and IRI + Nobiletin + ABX groups ($n = 8$ per group). Nobiletin was administered by oral gavage (50 mg/kg/day) for 14 days. In the IRI + Nobiletin + ABX group, mice were additionally treated with a daily oral dose of a broad-spectrum antibiotic cocktail (0.2 mL), consisting of ampicillin (5 mg/mL), gentamicin (5 mg/mL), neomycin (5 mg/mL), metronidazole (5 mg/mL), and vancomycin (2.5 mg/mL), for 14 consecutive days. Sham mice received the same volume of vehicle solution.

Folic acid model

Male mice were randomly divided into Control, FA, and FA + CS groups ($n = 8$ per group). The FA model was induced by intraperitoneal injection of Folic acid (250 mg/kg/day) for two consecutive days. Mice in the FA + CS group were pretreated with oral CS (0.2 mL, 10^8 CFU/mL) for 14 days, starting 12 days prior to model induction. Control mice received the same volume of vehicle.

Additional groups included Control, FA, FA + Nobiletin, and FA + Nobiletin + ABX ($n = 8$ per group). Nobiletin was administered orally at 50 mg/kg/day for 14 days. In the FA + Nobiletin + ABX group, mice received the same antibiotic cocktail described above, administered orally once daily for 14 consecutive days. Control mice received vehicle treatment on the same schedule.

Neutralization experiments

For the neutralization of IFN-γ experiments, anti-IFN-γ treatment group and isotype control group. Mice in the anti–IFN-γ group received an intraperitoneal injection of 300 μg anti–IFN-γ antibody (XMG1.2, Selleck Anti-mouse IFNγ-InVivo) after IRI. Mice in the isotype control group were administered the same dose of rat IgG2b isotype control (Rat IgG2b isotype control-InVivo, Selleck) via intraperitoneal injection on the same schedule.

ELISA assay

Sera were collected by centrifuging mouse blood samples at 3000 × g for 10 min. The supernatants were then used for the measurement of IFN-γ levels. The assay was performed using a commercial kit provided by Byabscience Biotechnology.

Fecal DNA extraction

Fecal DNA was extracted using the tianamp Stool DNA Kit according to the manufacturer's protocol. The primer sequences for 16s rRNA and functional genes are listed in Table 1.

Cell experiments

HK-2 cells were stimulated with 20 ng/mL IFN-γ in the presence of either IAA (100 μM) alone or a combination of IAA (100 μM) and CH-223191 (10 μg/mL) for 24 h. After treatment, the mRNA expression levels of *TNF-α*, *IL-1β*, *IL-6*, *AHR*, and *Cyp1A1* were detected.

Caco-2 cells were stimulated with 100 μg/mL lipopolysaccharide (LPS) in the presence of either IAA (100 μM) alone or a combination of IAA (100 μM) and CH-223191 (10 μg/mL) for 24 h. After treatment, cellular proteins were extracted, and the expression levels of ZO-1, Occludin, and AhR were analyzed by Western blotting.

Cultivation and preparation of CS bacterial cultures

Clostridium scindens ATCC 35704 were purchased from ATCC and cultivated in Chopped Meat Broth with Carbohydrates. An anaerobic chamber containing 10% CO_2, 10% H_2, and 80% N_2 was used for all anaerobic microbiological works. Cultures were collected in logarithmic phase and diluted with PBS to 2 × 10^8 CFU/mL for intragastric administration.

CS growth modulator in vitro screening

In a total volume of 4.5 mL CMC culture medium, 0.5 mL of *Clostridium scindens* bacterial suspension was inoculated. After inoculation, the culture was incubated under anaerobic conditions. Bacterial growth was monitored by measuring the optical density at 600 nm at various time points to construct a growth curve.

Standard compounds of Nobiletin and procyanidin were accurately weighed and dissolved in DMSO to prepare 100 mM stock solutions. These solutions were filtered through 0.22 μm sterile membranes prior to use and

Table 1 | 16s and CS primer sequence

Gene	Sequence
16 s	F: 5' - TGSTGCAYGGYTGTCGTCA- 3'
	R: 5' - ACGTCRTCCMCACCTTCCTC- 3'
C.scindens	F: 5' -GCATTTGGAACTGCGTGG- 3'
	R: 5' - CGTTACGCGCTTTGGCATCG - 3'

handled within an anaerobic glove box. For drug treatment groups, 4.5 mL of CMC medium, 500 μL of bacterial suspension, and 0.5 μL of stock solution (to achieve a final concentration of 10 μM) were added to screw-cap culture tubes and mixed thoroughly. The control group received an equivalent volume of DMSO without drug. All cultures were incubated under anaerobic and light-protected conditions.

At 12, 15, 20, 22, 24, 26, and 36 h after subculturing, 200 μL of culture medium from each group was transferred to a 96-well plate, and the absorbance at 600 nm was measured. Bacterial growth curves were generated using GraphPad Prism 8 and compared between treatment and control groups.

Serum biochemical analysis

Serum levels of blood urea nitrogen (BUN) and serum creatinine (Scr) were measured using a fully automated biochemical analyzer. The data were exported into Excel for statistical processing, and graphical representations were generated using GraphPad Prism 8.

Western blot analyses

Protein concentrations were determined using an enhanced BCA protein assay kit. Equal amounts of total protein were separated by SDS-polyacrylamide gel electrophoresis (SDS-PAGE) and transferred onto 0.45 μm hydrophobic polyvinylidene difluoride (PVDF) membranes. After transfer, membranes were blocked in 5% non-fat milk for 2 h at room temperature and then incubated overnight at 4 °C with the appropriate primary antibodies. The following day, membranes were washed and incubated with horseradish peroxidase (HRP)-conjugated secondary antibodies for 2 h at room temperature. The 10–20 μL of total protein was fractionated by Polyacrylamide gel and transferred to a 0.45 μm hydrophobic PVDF transfer membrane (IPVH00010, Merk Millipore, Germany). After incubated for 2 h in 5% non-fat milk blocking buffer, the membranes were incubated overnight at 4 °C with primary antibody. The following antibodies were used: anti-GAPDH (Proteintech Cat# HRP-60004, RRID:AB_2737588), anti-ZO-1(Proteintech Cat# 21773-1-AP, RRID:AB_10733242, Proteintech), anti-Occludin (Proteintech Cat# 66378-1-Ig, RRID:AB_2881755, Proteintec), anti-TNF-α (Abcam Cat# ab215188, RRID:AB_2935774,Abcam), anti-IL-6(Abcam Cat# ab259341, RRID:AB_2927381,Abcam), anti-NLRP3(Abcam Cat# ab263899, RRID:AB_2889890),anti-Caspase-1 (Proteintech Cat# 22915-1-AP, RRID:AB_2876874,Proteintech),anti-IL-1β(Cell Signaling Technology Cat# 12242, RRID:AB_2715503, HRP-linked anti-mouse IgG (Cell Signaling Technology Cat# 7076, RRID:AB_330924, CST, mouse). Cell Signaling Technology). Protein bands were visualized using chemiluminescence and analyzed semi-quantitatively using ImageJ software.

mRNA isolation and qPCR

Total mRNA was extracted using a High Pure RNA Isolation Kit (RNAiso Plus, Takara Bio, Japan) according to the manufacturer's instructions. Total RNA was reverse transcribed by a HiScript II QRT SuperMix for qPCR according to the manufacturer's instructions (+gDNA wiper, R233-01, Vazyme, Nanjing, China). qPCR was carried out by the StepOne System (A&B, Waltham, MA, USA) using AceQ qPCR SYBR Green Master Mix (High ROX Premixed, Q141-02, Vazyme Biotech Co. Ltd.). The amplification reaction procedure was: 95 °C, hold for 30 s; 95 °C 10 s, 60 °C, 30 s, 40 cycles. The mRNA levels of the genes were calculated by normalization to the levels of GAPDH. The primer sequences for all genes are listed in Table 2.

Protein microarray technology

Tissue samples were sectioned on dry ice, washed with cold PBS, and homogenized in RIPA buffer using a handheld homogenizer and ultrasonic disruption. After centrifugation at 13,200 rpm for 15 min at 4 °C, the supernatant was collected and stored at −80 °C overnight. The following day, samples were centrifuged again, and the clarified supernatant was transferred to a new tube for subsequent analysis by Huaying Biotechnology.

Table 2 | Primer sequences for all target genes

Gene	Sequence
Ifng	F: 5' - AAGACTGTGATTGCGGGGTT - 3'
	R: 5' - ATCTGAGTTCAGTCAGCCGC - 3'
AHR	F: 5' - GCCGGTGCAGAAAACAGTAAA - 3'
	R: 5' - AGCCAAACGGTCCAACTCTG - 3'
CYP1A1	F: 5'- CCCTTCTCAAATGTCCTGTAGTG -3'
	R: 5'- CAATGAGTTTGGGGAGGTTACTG-3'
Ahr	F: 5'- AGGCGGTCTAACTCTGTGTTC-3'
	R: 5'- CTGAAGTCAACCTCACCAGAAA-3'
Cyp1a1	F: 5'- CAGCCTTCCCAAATGGTTTA -3'
	R: 5'- GCCTGGGCTACACAAGACTC-3'
IL-1β	F: 5'-GCCAGTGAAATGATGGCTTATT-3'
	R: 5'-AGGAGCACTTCATCTGTTTAGG-3'
IL-6	F: 5'-CACTGGTCTTTTGGAGTTTGAG-3'
	R: 5'-GGACTTTTGTACTCATCTGCAC-3'
TNF-α	F: 5'-AGCTGGTGGTGCCATCAGAGG-3'
	R: 5'-TGGTAGGAGACGGCGATGCG -3'
GAPDH	F: 5'-GTCAAGGCTGAGAACGGGAA-3'
	R: 5'-AAATGAGCCCCAGCCTTCTC-3'
Gapdh	F: 5'-CCCTTATTGACCTCAACTACATGGT-3'
	R: 5'-GAGGGGCCATCCACAGTCTTCTG-3'

Untargeted metabolomics analysis of *Clostridium scindens* supernatants using Q-TOF

Untargeted metabolomics analysis of CS culture supernatants was performed using a quadrupole time-of-flight mass spectrometer (Q-TOF MS). For sample preparation, 500 μL of bacterial supernatant was mixed with 1500 μL of methanol, vortexed thoroughly, and incubated at 4 °C for 30 min. The mixture was then centrifuged at 13,200 rpm for 15 min at 4 °C. A volume of 1800 μL of the supernatant was transferred into a 2 mL EP tube, sealed with membrane film, punctured, and dried using a vacuum concentrator. The residue was reconstituted in 250 μL of 70% methanol–water, filtered through a 0.22 μm organic-phase membrane filter, and transferred into amber LC vials for analysis. The mobile phases consisted of 0.1% formic acid in ultrapure water (solvent A) and 0.1% formic acid in acetonitrile (solvent B). Chromatographic separation was carried out at 45 °C with a flow rate of 0.45 mL/min over a 23-minute gradient as follows: 0–1.5 min, 25% B; 1.5–3.5 min, 25–30% B; 3.5–6 min, 45% B; 6–10.5 min, 45–60% B; 10.5–13 min, 60–90% B; 13–14 min, 90–95% B; 14–16 min, 95–100% B; 16.5–18.5 min, 100% B; 18.5–22 min, 20% B; and 22–23 min, 20% B. The MS parameters were set as follows: gas temperature, 200°C; gas flow rate, 14 L/min; sheath gas temperature, 250°C; sheath gas flow rate, 11 L/min; and capillary voltage, 3000 V.

Targeted metabolomics analysis of *Clostridium scindens* supernatants

Targeted metabolomics analysis of CS culture supernatants was performed using a triple quadrupole mass spectrometer (QQQ). Standard solutions were prepared by accurately weighing 1 mg of each reference compound, dissolving in pure methanol, vortexing, sonicating for 5 min, and then diluting 1000-fold with methanol followed by filtration through a 0.22 μm organic-phase membrane. CS was cultured to the stationary phase and resuspended in PBS to a concentration of 2 × 10^8 CFU/mL. Cultures were supplemented with various precursors (D5-tryptophan, D5-indole-3-acetamide, D5-indole-3-pyruvate, or indole-3-acetaldehyde) and incubated anaerobically for 24 hours. After incubation, 500 μL of culture supernatant was mixed with 1500 μL of methanol, vortexed, incubated at 4 °C for 30 min, and centrifuged at 13,200 rpm for 15 min. Then, 1800 μL of the supernatant

was transferred into a 2 mL centrifuge tube, sealed with film, punctured, and dried using a vacuum concentrator. The residue was reconstituted in 250 μL of 70% methanol–water, filtered through a 0.22 μm organic membrane, and transferred to amber vials for analysis. Chromatographic separation was performed using a mobile phase of 0.1% formic acid in water (A) and 0.1% formic acid in acetonitrile (B) at a flow rate of 0.4 mL/min and a column temperature of 45 °C. The gradient elution over 16.5 minutes was as follows: 0–1.5 min, 10% B; 1.5–3.5 min, 20% B; 3.5–6 min, 20–30% B; 6–10.5 min, 30–45% B; 10.5–13 min, 45–100% B; 13–14 min, 100% B; 14–16 min, 100–20% B; and 16–16.5 min, 20–10% B. MS parameters were: gas temperature 200°C, gas flow 14 L/min, sheath gas temperature 250 °C, sheath gas flow 11 L/min, and capillary voltage 3000 V.

LC-MS/MS quantification of Indole-3-Acetic Acid in serum and Fece

IAA concentrations in mouse feces and serum were measured using a triple quadrupole mass spectrometer (QQQ). Standard solutions were prepared by dissolving 1 mg of IAA in pure methanol, followed by vortexing, sonication for 5 minutes, 1000-fold dilution with methanol, and filtration through a 0.22 μm organic-phase membrane filter. For serum samples, 100 μL of serum was mixed with 400 μL of acetonitrile, vortexed, sonicated, and centrifuged at 12,000 rpm for 10 min. The supernatant was transferred into an EP tube, dried after sealing and puncturing, and reconstituted in 400 μL of 80% acetonitrile-water. After further vortexing and sonication for 5 min, samples were filtered through a 0.22 μm membrane. For fecal samples, 30 mg of feces was homogenized with 400 μL of 70% methanol–water, sonicated, and centrifuged at 13,000 rpm for 10 minutes. The supernatant was dried in a sealed, punctured EP tube, reconstituted in 360 μL of 70% methanol–water, and filtered through a 0.22 μm membrane. Chromatographic separation was conducted under the same conditions as described above, using 0.1% formic acid in water (A) and 0.1% formic acid in acetonitrile (B) at a flow rate of 0.4 mL/min and a column temperature of 45 °C, with the identical gradient elution procedure. MS acquisition parameters were: gas temperature 200 °C, gas flow rate 14 L/min, sheath gas temperature 250 °C, sheath gas flow rate 11 L/min, and capillary voltage 3000 V.

Data availability

The data that support the findings of this study are available from the corresponding author upon reasonable request.

Received: 3 July 2025; Accepted: 1 December 2025;
Published online: 15 December 2025

References

1. Ostermann, M. et al. Acute kidney injury. *Lancet* **405**, 241–256 (2025).
2. Vijayan, A. Tackling AKI: prevention, timing of dialysis and follow-up. *Nat. Rev. Nephrol.* **17**, 87–88 (2021).
3. Guo, R. et al. The Road from AKI to CKD: Molecular Mechanisms and Therapeutic Targets of Ferroptosis. *Cell Death Dis.* **14**, 426 (2023).
4. Gong, J., Noel, S., Pluznick, J. L., Hamad, A. R. A. & Rabb, H. Gut Microbiota-Kidney Cross-Talk in Acute Kidney Injury. *Semin. Nephrol.* **39**, 107–116 (2019).
5. Zhou, W. et al. The gut microbe Bacteroides fragilis ameliorates renal fibrosis in mice. *Nat. Commun.* **13**, 6081 (2022).
6. Si, Z. L. et al. Gut Bacteroides ovatus ameliorates renal fibrosis by promoting the production of HDCA through upregulation of Clostridium scindens. *Cell Rep.* **43**, 114830 (2024).
7. Chou, Y. T., Kan, W. C. & Shiao, C. C. Acute Kidney Injury and Gut Dysbiosis: A Narrative Review Focus on Pathophysiology and Treatment. *Int. J. Mol. Sci.* **23**, https://doi.org/10.3390/ijms23073658 (2022).
8. Meng, Y. et al. Bifidobacterium bifidum alleviates adenine-induced acute kidney injury in mice by improving intestinal barrier function. *Food Funct.* **15**, 8030–8042 (2024).
9. Zhu, X. X. et al. Gut microbiome and metabolites mediate the benefits of caloric restriction in mice after acute kidney injury. *Redox Biol.* **77**, 103373 (2024).
10. Yang, Z. et al. The prevention effect of Limosilactobacillus reuteri on acute kidney injury by regulating gut microbiota. *Microbiol. Immunol.* **68**, 213–223 (2024).
11. Xiao, J. et al. Clostridium Scindens Protects Against Vancomycin-Induced Cholestasis and Liver Fibrosis by Activating Intestinal FXR-FGF15/19 Signaling. *Adv. Sci. (Weinh., Baden.-Wurtt., Ger.)* **12**, e2406445 (2025).
12. Saenz, C. et al. Clostridium scindens secretome suppresses virulence gene expression of Clostridioides difficile in a bile acid-independent manner. *Microbiol. Spectr.* **11**, e0393322 (2023).
13. Agus, A., Planchais, J. & Sokol, H. Gut Microbiota Regulation of Tryptophan Metabolism in Health and Disease. *Cell Host Microbe* **23**, 716–724 (2018).
14. Moro, K. et al. Interferon and IL-27 antagonize the function of group 2 innate lymphoid cells and type 2 innate immune responses. *Nat. Immunol.* **17**, 76–86 (2016).
15. González-Navajas, J. M., Lee, J., David, M. & Raz, E. Immunomodulatory functions of type I interferons. *Nat. Rev. Immunol.* **12**, 125–135 (2012).
16. Li, M. et al. Gut microbiota metabolite indole-3-acetic acid maintains intestinal epithelial homeostasis through mucin sulfation. *Gut Microbes* **16**, 2377576 (2024).
17. Huang, W. et al. Nobiletin protects against ferroptosis to alleviate sepsis-associated acute liver injury by modulating the gut microbiota. *Food Funct.* **14**, 7692–7704 (2023).
18. Li, L. et al. Perspective on the Modern Interpretation of the Property Theory of Mild-natured and Sweet-flavored Traditional Chinese Medicine via Gut Microbiota Modulation. *Integr. Med. Nephrol. Androl.* **10**, e00012 (2023).
19. Wang, Q., Li, J. & Chen, L. Traditional Chinese Medicine Phytochemicals: Promising Therapeutic Agents for Acute Kidney Injury. *Integr. Med. Nephrol. Androl.* **12**, e25–00037 (2025).
20. Yang, J. et al. Intestinal microbiota control acute kidney injury severity by immune modulation. *Kidney Int.* **98**, 932–946 (2020).
21. Park, S. W. et al. Cytokines induce small intestine and liver injury after renal ischemia or nephrectomy. *Lab Invest* **91**, 63–84 (2011).
22. Guerrero-Mauvecin, J. et al. Regulated necrosis role in inflammation and repair in acute kidney injury. *Front Immunol.* **14**, 1324996 (2023).
23. Wang, H. et al. Perturbed gut microbiome and fecal and serum metabolomes are associated with chronic kidney disease severity. *Microbiome* **11**, 3 (2023).
24. Wang, J. et al. Inulin Supplementation Alleviates Ochratoxin A-Induced Kidney Injury through Modulating Intestinal Microbiota. *J. Agric Food Chem.* **72**, 18682–18696 (2024).
25. Zeng, Y. et al. Gut microbiota-derived indole-3-propionic acid alleviates diabetic kidney disease through its mitochondrial protective effect via reducing ubiquitination mediated-degradation of SIRT1. *J. Adv. Res.* https://doi.org/10.1016/j.jare.2024.08.018 (2024).
26. Meibom, K. L. et al. BaiJ and BaiB are key enzymes in the chenodeoxycholic acid 7α-dehydroxylation pathway in the gut microbe Clostridium scindens ATCC 35704. *Gut Microbes* **16**, 2323233. https://doi.org/10.1080/19490976.2024.2323233 (2024).
27. Greathouse, K. L., Harris, C. C. & Bultman, S. J. Dysfunctional families: Clostridium scindens and secondary bile acids inhibit the growth of Clostridium difficile. *Cell Metab.* **21**, 9–10 (2015).
28. Du, W. et al. The microbiota-dependent tryptophan metabolite alleviates high-fat diet-induced insulin resistance through the hepatic AhR/TSC2/mTORC1 axis. *Proc. Natl. Acad. Sci. USA* **121**, e2400385121 (2024).
29. Rocha, C. S. et al. Microbial remodeling of gut tryptophan metabolism and indole-3-lactate production regulate epithelial barrier repair and

viral suppression in human and simian immunodeficiency virus infections. *Mucosal Immunol*. https://doi.org/10.1016/j.mucimm.2025.01.011 (2025).
30. Ding, Y. et al. Oral supplementation of gut microbial metabolite indole-3-acetate alleviates diet-induced steatosis and inflammation in mice. *Elife* **12**. https://doi.org/10.7554/eLife.87458 (2024).
31. Pernomian, L., Duarte-Silva, M. & de Barros Cardoso, C. R. The Aryl Hydrocarbon Receptor (AHR) as a Potential Target for the Control of Intestinal Inflammation: Insights from an Immune and Bacteria Sensor Receptor. *Clin. Rev. Allergy Immunol.* **59**, 382–390 (2020).
32. Schiering, C. et al. Feedback control of AHR signalling regulates intestinal immunity. *Nature* **542**, 242–245 (2017).
33. Li, Y. Y. et al. Baicalein ameliorates ulcerative colitis by improving intestinal epithelial barrier via AhR/IL-22 pathway in ILC3s. *Acta Pharm. Sin.* **43**, 1495–1507 (2022).
34. Fu, B. et al. SEPTIN2 suppresses an IFN-γ-independent, proinflammatory macrophage activation pathway. *Nat. Commun.* **14**, 7441 (2023).
35. Lu, X. et al. A20 in Myeloid Cells Protects Against Hypertension by Inhibiting Dendritic Cell-Mediated T-Cell Activation. *Circ. Res.* **125**, 1055–1066 (2019).
36. Ji, J. et al. Interferon-γ-Induced Myeloid-Derived Suppressor Cells Aggravate Kidney Ischemia-Reperfusion Injury by Regulating Innate Immune Cells. *Nephron* **146**, 99–109 (2022).
37. Li, L. et al. IL-17 produced by neutrophils regulates IFN-gamma-mediated neutrophil migration in mouse kidney ischemia-reperfusion injury. *J. Clin. Invest* **120**, 331–342 (2010).
38. Yu, T. et al. Colon-targeted engineered postbiotics nanoparticles alleviate osteoporosis through the gut-bone axis. *Nat. Commun.* **15**, 10893 (2024).

Acknowledgements

This work was financially supported by the National Natural Science Foundation of China (32560025 to Z.-H.Z., 82160135 and 82360146 to J.-L.W.), Hainan Provincial Natural Science Foundation of China (Grants 825MS069 to Z.-H.Z.), Excellent Talent Team Project in Hainan Province (HNYT20250004 to Z.-H.Z.), Hainan key research and development projects (ZDYF2025SHFZ041 to J.-L.W.), the CACMS Innovation Fund (No. CI2024E003KC-02 to Y.L.), the Fundamental Research Funds for the Centralpublic welfare research institutes (Nos. ZXKT21021, ZXKT23011 to Y.L.), Academic Enhancement Program of Hainan Medical University (XSTS2025102 to J.-L.W.) and Hainan Province Clinical Medical Center.

Author contributions

Z.-H.Z. and J.-L. W designed and managed experiments. Y.-Z.C., J.-Y.Li., K.-S. and J.-M.H. collected and analyzed the data. Y.-Z.C., J.-Y.Li., J.-M.H., and J.-L.C. conducted animal and cell experiments. Z.-H.Z. and Y.-Z.C. wrote the manuscript. Z.-H.Z., and Y.L. contributed to text revision and discussion.

Competing interests

The authors declare no competing interests.

Additional information

Supplementary information The online version contains supplementary material available at https://doi.org/10.1038/s41522-025-00884-7.

Correspondence and requests for materials should be addressed to Zhi-hao Zhang.